See discussions, stats, and author profiles for this publication at: https://www.researchgate.net/publication/231240901

## Li 2FeSiO 4 polymorphs probed by 6Li MAS NMR and 57Fe Mössbauer spectroscopy

ARTICLE in CHEMISTRY OF MATERIALS · MAY 2011

Impact Factor: 8.35 · DOI: 10.1021/cm103193a

**CITATIONS READS** 

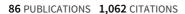
33

**5 AUTHORS**, INCLUDING:



#### **Gregor Mali**

National Institute of Chemistry - Kemijski in..



SEE PROFILE



## Darko Hanzel

Jožef Stefan Institute

83 PUBLICATIONS 1,568 CITATIONS

SEE PROFILE



83

## **Christian Masquelier**

Université de Picardie Jules Verne

165 PUBLICATIONS 7,300 CITATIONS

SEE PROFILE



## **Robert Dominko**

National Institute of Chemistry

132 PUBLICATIONS 4,596 CITATIONS

SEE PROFILE

# <sup>6</sup>Li MAS NMR and <sup>57</sup>Fe Mössbauer spectroscopy characterisation of

## Li<sub>2</sub>FeSiO<sub>4</sub> polymorphs

*Gregor Mali*<sup>a,b</sup>, *Chutchamon Sirisopanaporn*<sup>a,c,d</sup>, *Christian Masquelier*<sup>c,d</sup>, *Darko Hanzel*<sup>e</sup>,

Robert Dominko<sup>a,d</sup>

<sup>a</sup> National Institute of Chemistry, P.O.B. 660, SI-1001 Ljubljana, Slovenia

<sup>b</sup> EN-FIST Centre of Excellence, Dunajska 156, SI-1000 Ljubljana, Slovenia

<sup>c</sup> LRCS, Université de Picardie Jules Verne, 33 Rue Saint-Leu, 80039 Amiens, France

<sup>d</sup> ALISTORE-ERI, 80039, 33 Rue Saint-Leu, Amiens Cedex, France

<sup>e</sup> Jozef Stefan Institute, Jamova 39, SI-1000 Ljubljana, Slovenia

**Keywords:** Mössbauer spectroscopy, MAS NMR, DFT/GIPAW, Li<sub>2</sub>FeSiO<sub>4</sub>, Li-ion batteries

#### **Abstract:**

Several samples of pure Li<sub>2</sub>FeSiO<sub>4</sub> polymorphs, prepared by hydrothermal synthesis and then quenched from  $400^{\circ}$ C  $(Pmn2_1)$ ,  $700^{\circ}$ C  $(P2_1/n)$  and  $900^{\circ}$ C (Pmnb), were thoroughly investigated by Mössbauer and NMR spectroscopy. <sup>57</sup>Fe Mössbauer spectroscopy showed that the iron in all the polymorphs was in the divalent oxidation state, and that chemical shifts and quadrupolar splitting correlated well with Fe-O bond-lengths, respectively. <sup>6</sup>Li MAS NMR spectra of three different polymorphs exhibit substantially different spinning-sideband patterns and slightly different isotropic shifts. The sideband patterns stemming from the anisotropic electron-nucleus dipole-dipole interaction reflects the arrangement of paramagnetic iron ions around lithium nuclei and allowed unambiguous assignments of <sup>6</sup>Li MAS NMR signals to crystallographically inequivalent Li sites. Analysis of isotropic NMR shifts of <sup>6</sup>Li nuclei revealed that they comprised two contributions of comparable magnitude, a hyperfine (contact) shift and a pseudo-contact shift. Based on the structural models of Li<sub>2</sub>FeSiO<sub>4</sub> polymorphs, both contributions could be successfully predicted by first-principles calculations. The contact shift was obtained from the hyperfine-coupling constant on <sup>6</sup>Li nuclei, which was calculated within a DFT/PAW approach, and the pseudo-contact shift was derived from the electron-nucleus dipolar matrix and the g-tensor, which was computed within the DFT/GIPAW frame.

#### Introduction

The interest in polyanionic materials as positive electrode materials for Li-ion batteries has increased dramatically after the first report on the electrochemical activity of LiFePO<sub>4</sub> [1]. Oxygen atoms in the polyanionic framework structures are stabilized by X-O bonds (X=P, Si, B,...) with a strong covalent nature. This makes polyanionic-based materials safer and more stable over prolonged cycling. The most attractive member of this group is Li<sub>2</sub>FeSiO<sub>4</sub> (LFS) [2-3], which offers the possibility for a cheap cathode material due to abundant raw materials. In the recent works, where small particles of LFS and proper electrode engineering have been used, almost theoretically predicted capacity and good cycling stability were achieved [4-5]. In addition to the challenges of enhancing the electrochemical performance, an important part of the research is also devoted to the accurate description of the structure of LFS, more precisely to the elucidation of the structural differences between the polymorphs of LFS and to the understanding of the importance of these differences. Several polymorphs were recently isolated and characterized based on the careful study by X-ray and Neutron diffractions as well as transmission electron microscopy [6-8]. The proposed structural models for LFS were derived from Li<sub>3</sub>PO<sub>4</sub> structures and can be roughly divided into two large subgroups, a low temperature group [9] denoted as  $\beta$  group, and a high temperature group [10] denoted as  $\gamma$ group. In both structural models half of tetrahedral sites, generated by a distorted hexagonal close packing of oxygen atoms, are occupied by cations, and the difference is in the respective orientations of the filled tetrahedra and in their connectivity.

The above described differences among the LFS polymorphs are generally observed in well crystalline samples, while in the samples prepared for the electrochemical characterization (with particles below 50 nm) or in the samples where a mixture of polymorphs is present, low quality of the powder X-ray diffraction patterns may not enable a reliable determination of the structure. In such cases characterization techniques that can detect local environments of

cations in the samples (for instance, NMR or Mössbauer spectroscopy) are much more informative.

Important parameters, like isomer shift (IS) and quadrupole splitting (QS), can be derived from Mössbauer spectra and can provide information about iron coordination, valence state and covalency of the iron-ligand bonds. It is generally accepted that for a given oxidation state and for identical ligands, an increase in the covalency of the iron-ligands bonds corresponds to a decrease in the iron-ligands interatomic distances which is translated into an observed decrease in the isomer shift [11].

Nuclear magnetic resonance (NMR) spectroscopy has been used as a characterization technique for many lithium-containing materials for Li batteries [12]. Lithium NMR spectroscopy was particularly useful for the elucidation of structural motifs that did not exhibit long-range order and thus could not be analyzed by diffraction techniques [13-15]. Recently, MAS NMR spectroscopy of <sup>6</sup>Li nuclei has proved to be a very convenient tool that could distinguish between different Li<sub>2</sub>MnSiO<sub>4</sub> polymorphs [16]. Lithium nuclei within polymorphs of Li<sub>2</sub>MnSiO<sub>4</sub> or lithium nuclei occupying crystallographically inequivalent lithium sites within a single polymorph exhibited NMR signals at different and well resolved isotropic positions.

Several structural issues related to tetrahedral lithium-containing transition metal silicates or phosphates have been studied also by first-principles calculations [17-20]. For example, density-functional theory (DFT) based calculations were able to predict the stability of pure Li<sub>2</sub>MnSiO<sub>4</sub> polymorphs [17] and of the Li<sub>2</sub>Fe<sub>z</sub>Mn<sub>(1-z)</sub>SiO<sub>4</sub> solid-solutions [20]. In many cases first-principles calculations also helped in the interpretation of NMR spectra, in particular related to the isotropic shifts detected in <sup>6</sup>Li or <sup>7</sup>Li NMR spectra [21-23]. Since isotropic shifts are governed by the magnitude of hyperfine coupling between the magnetic moments of the unpaired electronic spins and the nuclear magnetic moments of <sup>6</sup>Li or <sup>7</sup>Li nuclei, the accuracy

of predictions depends predominantly on the accuracy of the determination of electronic spin density at the position of the above-mentioned nuclei. It was shown that very good predictions of hyperfine coupling constants and isotropic shifts could be obtained by using DFT, pseudopotentials and Projector Augmented-Wave (PAW) approach [16, 24].

In this work we have used <sup>57</sup>Fe Mössbauer spectroscopy and <sup>6</sup>Li solid-state MAS NMR spectroscopy to investigate Li<sub>2</sub>FeSiO<sub>4</sub> polymorphs. A systematic study on several samples prepared at different temperatures has been performed. The analysis of NMR spectra has been complemented by first principles calculations of hyperfine coupling constants and elements of the *g*-tensor. The obtained results are correlated with the structural models determined in our recent publications [7, 8]. The knowledge about the local structure of the Li<sub>2</sub>FeSiO<sub>4</sub> polymorphs, and about the spectroscopic methods to investigate this structure, has been used for the characterization of a typical carbon-coated Li<sub>2</sub>FeSiO<sub>4</sub> sample prepared at 700°C and slowly cooled down to room temperature.

## **Experimental**

Different LFS polymorphs were prepared by annealing pristine hydrothermally prepared LFS samples in the sealed stainless steel tubes filled with argon atmosphere. The samples were heated for 6 hours at selected temperatures (400°C, 700°C and 900°C) and quenched to 25°C. The detailed synthesis procedure is described in [8]. The typical sample for the electrochemical characterisation was prepared by mixing citric acid (1.3g) and as-prepared hydrothermal sample (1g). It was heat treated at 700°C in CO/CO<sub>2</sub> atmosphere for 6 hours and slowly cooled down to room temperature.

The powder X-ray diffraction patterns of as prepared LFS polymorphs were measured using  $CuK_{\alpha 1,2}$  radiation at 298 K. The machine was equipped with a LinxEye detector that allows energy discrimination (to remove part of the fluorescence). The data were recorded in the 20

range between 10 and 90° with a 20 step size of approximately  $0.02^{\circ}$  and with a constant counting time of 12 s per step. The patterns were analyzed by full pattern matching and Rietveld refinements as implemented in the Fullprof program [25].

<sup>57</sup>Fe Mossbauer experiments were performed in the transmission geometry at 298 K. The source was <sup>57</sup>Co in a Rh matrix. Velocity calibration and isomer shifts (IS) were quoted relative to an absorber of metallic iron at room temperature. Parameter fits were performed using a standard least-squares fitting routine with Lorentzian lines.

Differential thermal analysis was performed between 25 to 950 °C under constant flow of Argon using a Simultaneous Thermal Analyzer STA 449 °C Jupiter® from Netzsch, and a heating/cooling rate of 10 °Cmin<sup>-1</sup>.

Solid-state <sup>6</sup>Li magic-angle spinning (MAS) NMR spectra were recorded on a 600 MHz Varian NMR system, operating at <sup>6</sup>Li Larmor frequency of 88.274 MHz, with rotation synchronized Hahn-echo pulse sequence. Sample rotation frequency was 20 kHz, repetition delay between consecutive scans was 0.1 s and number of scans was 15 000. Frequency axis in ppm is reported relative to the lithium signal of 1M solution of LiCl. Spinning-sideband powder patterns were analyzed by Spinevolution simulation package [26] and 'dmfit' software [27]. In addition to electron-nucleus dipolar interaction, electric quadrupolar interaction was also considered when fitting the spectra of <sup>6</sup>Li nuclei.

First-principles calculations were performed using the density functional theory (DFT) in the generalized gradient approximation of Perdew-Burke-Ernzerhof (GGA PBE) [28] with plane wave basis and norm-conserving pseudopotentials. In the first step the atomic coordinates of atoms within LFS polymorphs were relaxed and optimized with Quantum Espresso's *pwscf* program [29]. The 'final' ground state energies were then recalculated with the optimized geometries. In all calculations plane-wave cutoff energy was 1360 eV. The reciprocal-space sampling was performed with *k*-point grids of 4x4x4 points. All-electron information was

reconstructed using the Projector Augmented-Wave (PAW) [16, 24] and Gauge-Including Projector Augmented-Wave (GIPAW) [30, 31] methods as implemented in Quantum Espresso's *GIPAW* module [29]. The module yielded hyperfine coupling constants and elements of *g*-tensors, which were then used for quantitative prediction of the isotropic shifts.

#### **Results and discussion**

In our recent works [7, 8] we showed that at least three polymorphs of Li<sub>2</sub>FeSiO<sub>4</sub> can be isolated through careful quenching procedures. A stoichiometric sample without impurities prepared by hydrothermal synthesis can serve as a good starting point for the isolation of different LFS polymorphs at different temperatures. Thermogravimetric data (Figure 1a) showed a small loss of mass in the temperature range up to 300°C, related to the desorption of physically and chemically adsorbed water [32]. The reason for the additional loss of mass in the temperature range between 700°C and 800°C is not clear at the present stage. More important information is obtained from the DSC data (Figure 1b), where exothermic peaks during heating and endothermic peaks during cooling clearly delimit the stability ranges of the three polymorphs. The DSC diagram upon heating displays a steep curve due to the agglomeration of small initial particles, which hinders the possibility of precise determination of the phase transition enthalpies. The low temperature polymorph  $\beta$  ( $Pmn2_1$ ) transforms into the high temperature polymorph  $\gamma_s$  (P2<sub>1</sub>/n) at a temperature around 530°C. The phase transition temperature from  $\gamma_s$  to  $\gamma_{II}$  (*Pmnb*) polymorph was determined to be close to 875 °C upon heating. The phase transitions are reversible throughout the cooling process with the temperature around 724 °C for transition from  $\gamma_{II}$  to  $\gamma_{s}$ , and around 453 °C for transition from  $\gamma_s$  to  $\beta$ . Using the DSC data we have isolated three different samples by quenching as prepared hydrothermal samples sealed in stainless steel tube filled with Ar from 400 °C (LFS@400), 700 °C (LFS@700) and 900 °C (LFS@900) to 25 °C.

All samples were checked by Rietveld refinement of powder X-ray diffraction patterns. The refinements of LFS@700 and LFS@900 were based on the structural models that were recently reported in the literature [6-8] and are given in the supplementary information file. The structural model for LFS@400 was obtained using the coordinates of β-Li<sub>3</sub>PO<sub>4</sub> and Li<sub>2</sub>MnSiO<sub>4</sub> [3, 33]. The calculated vs. experimental plots are given in Figure 2, the atomic coordinates, lattice parameters and reliability factors are given in Table1 and the bond lengths and angles in Table2.

A close look at the local environments of Fe<sup>2+</sup> in each polymorph reveals interesting differences. In all polymorphs, divalent iron atoms are in tetrahedral coordination, surrounded by two LiO<sub>4</sub> tetrahedra and by one SiO<sub>4</sub> tetrahedron. The differences between iron environments are in the connectivity and in the orientations of the tetrahedra. In the sample crystallized within Pmn21 space group (LFS@400) all tetrahedra share corners, and they are all pointing in the same direction along c axis (Figure 3a). The structures of the high temperature polymorphs (LFS@700 and LFS@900) are more complicated. In the  $P2_1/n$ (LFS@700) phase FeO<sub>4</sub> shares one edge with LiO<sub>4</sub> tetrahedron (Figure 3b), whereas in the Pmnb one (LFS@900) FeO<sub>4</sub> shares two edges with LiO<sub>4</sub> tetrahedra (Figure 3c). The orientation of tetrahedra in the high temperature polymorphs alternates in their pointing direction: up-up-down-down-up-up-down-down for P21/n structure (LFS@700) and updown-up-down-up-down for Pmnb structure (LFS@900). The alternation of Fe and Si (Fe-Si-Fe-Si-Fe) is common for all three structures. Differences in the tetrahedra connectivity and in the orientation have an influence on the average bond length in the FeO<sub>4</sub> tetrahedra. The general trend observed is the decrease in the average Fe-O bond length from LFS@400 to LFS@900 polymorphs. The largest average bond length between oxygen and iron was found in the LFS@400 sample (2.076(4) Å) and the smallest in the LFS@900 sample (2.026(1) Å), while the average bond length in the LFS@700 sample was 2.032(1) Å. Based on the crystallographic data an opposite correlation was determined for the distortion [34] of FeO<sub>4</sub> tetrahedra. The largest distortion was found in LFS@900 sample ( $12.8 \times 10^{-4} \text{ Å}^3$ ) and the smallest in LFS@400 sample ( $2.3 \times 10^{-4} \text{ Å}^3$ ), while the distortion in the LFS@700 sample was  $9.9 \times 10^{-4} \text{ Å}^3$  [35].

## Mössbauer spectroscopy

Those significant variations in the local environments of FeO<sub>4</sub> tetrahedra among all Li<sub>2</sub>FeSiO<sub>4</sub> polymorphs can be addressed through Mössbauer spectroscopy, as previously reported for iron oxides and iron fluorides [11]. Figure 4 shows the Mössbauer spectra of the three polymorphs used in this work. The measurements confirmed the high quality of the samples; i.e. the samples do not contain any detectable trace of Fe<sup>III</sup> or other Fe<sup>II</sup> – containing oxides, contrary to what had been reported by Thomas et al. [2]. Parameters (isomer shift and quadrupole splitting) of fitted spectra are within the ranges commonly observed for Fe in tetrahedral coordination [11] but are significantly different from one sample to the other. Noticeably, each spectrum could be fitted nicely ( $\chi^2$  within  $3\sigma$  range) with only one contribution from Fe, in full accordance with the crystal structures of the three polymorphs, each of them comprising only one Fe crystallographic site.

Interestingly, the respective chemical shifts of the three samples follow a general trend observed in other systems [11]: the increase in the covalent nature of the Fe-O bond (decrease in the average bond length) translates into a smaller chemical shift, from 0.93 mm.s<sup>-1</sup> (LFS@900) to 0.97 mm.s<sup>-1</sup> (LFS@400) (Figure 4). Those observations were validated for many samples and are reproducible (Figure 5).

Even larger differences between samples were observed when comparing the quadrupole splitting values which can be strongly correlated to the degree of the distortion of the FeO<sub>4</sub> tetrahedra, as reported by Dyar et al. for Fe in staurolite samples [36]. The trend of smaller

quadrupole splitting for a higher distortion, observed here, cannot be taken as a general one in Mössbauer spectroscopy but can be used in a particular system where  $Fe^{2+}$  have the same type and number of ligands.

## <sup>6</sup>Li MAS NMR

As in our recent work on Li<sub>2</sub>MnSiO<sub>4</sub> [16] we measured the <sup>6</sup>Li MAS NMR spectra on different Li<sub>2</sub>FeSiO<sub>4</sub> polymorphs in order to strengthen the information about the local structure, gathered so far through diffraction (electron, X-Ray, neutron) and Mössbauer spectroscopy. The NMR spectra of LFS@400, LFS@900, and LFS@700 are shown in Figure 6. All three spectra exhibit broad spinning-sideband patterns reflecting strong anisotropic dipolar interactions of lithium nuclei with electronic spins of paramagnetic centres which are predominantly iron ions (and in a smaller extent if electronic spins are partly delocalized, also ions of oxygen). Compared to lithium NMR signals of Li<sub>2</sub>MnSiO<sub>4</sub> polymorphs, individual centrebands and sidebands in spectra of LFS polymorphs are approximately 10 times broader. While the FWHM of the former was about 6 to 7 ppm, FWHM of the latter is approximately 60 to 70 ppm. The difference in linewidths cannot be attributed to different relaxation rates, because <sup>6</sup>Li T<sub>2</sub> relaxation times of all Li<sub>2</sub>MnSiO<sub>4</sub> and Li<sub>2</sub>FeSiO<sub>4</sub> polymorphs are almost the same; they are approximately 3 ms long and correspond to linewidths of approximately one ppm. The much stronger broadening of the centrebands and sidebands in the spectra of Li<sub>2</sub>FeSiO<sub>4</sub> must thus be produced by another mechanism, most probably by the anisotropic bulk magnetic susceptibility effect, as discussed later in the text.

LFS@400 and LFS@900 samples both exhibit a single lithium contribution with isotropic positions of -72 and -30 ppm, respectively. This is consistent with the proposed crystal structures for *Pmn2*<sub>1</sub> (LFS@400 sample) and *Pmnb* (LFS@900 sample) polymorphs, which both contain a single lithium site within their asymmetric crystallographic units. On the other

hand, the spectrum of LFS@700 can be decomposed into two equally strong contributions (intensity ratio of 0.49:0.51). The isotropic positions of the two contributions are -7 and -55 ppm, as previously mentioned by G. Quoirin [37]. Because of large linewidths, the two contributions severely overlap, yielding slightly asymmetric NMR centreband and sidebands. Perhaps easier to rationalize than the difference in isotropic positions of the two lithium contributions is the difference in widths of their spinning-sideband patterns (see Figure 7). As already mentioned, the width of the sideband pattern depends on the magnitude of the dipolar interaction of lithium nuclei with paramagnetic centres, which in turn depends on the distances between the nuclei and the centres. Inspecting the proposed structure of  $P2_1/n$ polymorph, [38] one can distinguish two equally populated lithium sites. While the Li(2)O<sub>4</sub> tetrahedron shares corners with four neighbouring FeO<sub>4</sub> tetrahedra, the Li(1)O<sub>4</sub> tetrahedron shares corners with two and an edge with one of the neighbouring FeO<sub>4</sub> tetrahedra (see Figure 3). The distances between lithium and iron sites in edge-sharing tetrahedra are substantially shorter than the distances between lithium and iron sites in corner-sharing tetrahedra. The first amount to approximately 0.28 nm and the second exceeds 0.3 nm. Because of the short distance, the interaction between Li(1) nuclei and iron centres is stronger, and the induced width of the NMR spinning-sideband powder pattern is larger. Tentatively, a narrower powder pattern with isotropic shift of -55 ppm can be assigned to the Li(2) site, and a broader powder pattern with isotropic shift of -7 ppm can be assigned to the Li(1) site.

The width and the shape of the spinning-sideband powder patterns can be assessed also more quantitatively. It was shown by Nayeem and Yesinowski [39] that the effect of through-space dipolar interaction between the nuclear spin and several paramagnetic centres can be described by the hamiltonian

$$H_{en} = \hbar \gamma \ \boldsymbol{B}_0 \cdot \boldsymbol{\sigma}_{en} \cdot \boldsymbol{I} , \qquad (1)$$

where  $\gamma$  is nuclear gyromagnetic ratio,  $\boldsymbol{B}_0$  is external magnetic field, and  $\boldsymbol{I}$  is nuclear spin operator. Tensor  $\boldsymbol{\sigma}_{en}$  can be expressed as

$$\boldsymbol{\sigma}_{en} = \frac{\mu_0}{4\pi} \frac{\mu_B^2 S(S+1)}{3kT} \quad \boldsymbol{g} \cdot \boldsymbol{g} \cdot \boldsymbol{D}_{en} . \tag{2}$$

Here  $\mu_B$  is Bohr magneton, S is spin of the paramagnetic centre, and  $D_{en}$  is the dipolar matrix  $\left(D_{\alpha\beta} = \sum_i (\delta_{\alpha\beta} - 3e_{\alpha}^i e_{\beta}^i)/r_i^3\right)$ , which contains only information about the positions of paramagnetic centres with respect to the nucleus. Other symbols have their usual meaning. If we take the g tensor to be isotropic and equal to 2, we can verify if meaningful prediction of the spinning-sideband powder patterns of  $^6$ Li MAS NMR spectra can be obtained solely based on the geometrical information about the arrangement of Fe<sup>2+</sup> ions around Li nuclei. We calculated the  $\sigma_{en}$  tensors for lithium sites of  $P2_1/n$ ,  $Pmn2_1$  and Pmnb polymorphs using the proposed structures and assuming that spin-delocalization is negligible. We took into account all the Fe sites within the sphere of radius of 0.8 nm around a selected Li nucleus and estimated the effective magnetic moment by theoretical Bohr magneton number for Fe<sup>2+</sup> ions of 4.9 [40], anticipating that crystal field was much stronger than spin-orbit coupling.

The calculated anisotropy parameters  $\sigma_{en}^{aniso}$  are compared to the experimentally obtained ones in Figure 8. The latter anisotropy parameters were actually extracted from  $^6$ Li MAS NMR spectra by the simulations of spinning-sideband patterns (see Supplementary material). In addition to interaction with paramagnetic centres, the sideband patterns of  $^6$ Li MAS NMR spectra are affected also by electric quadrupolar interaction [41]. Chemical shift anisotropy and nuclear dipole-dipole couplings are negligible and were not taken into account in the analysis of the sideband patterns. We also did not take into account the bulk magnetic susceptibility (BMS) effect. In diamagnetic materials broadening due to BMS is usually rather small and is spun away by magic angle spinning [42,43]. In paramagnetic materials, however, the BMS effect can be large and often cannot be entirely removed by MAS. In some cases it

can contribute substantially to sideband intensities [41]. Quantitatively the BMS contribution to spinning-sideband pattern is, unfortunately, very difficult to assess, and its analysis exceeds the scope of this paper.

The results of the analysis of sidebands patterns, taking into account only electron-nucleus dipolar and electric quadrupolar interactions, are collected in Table 3. The above mentioned approximations, especially the neglected BMS effect, might be responsible for the slight disagreement between the measured and the simulated NMR spectra (see Supplementary material). Because of that, the anisotropy parameters extracted by the analysis of spinningsideband intensities can be considered more as the estimates than as the precisely measured values. Nevertheless, they still correlate well with the predicted anisotropy parameters and can be rationalized by the differences in the symmetry of the local Li environments. The Li site of  $Pmn2_1$  and Li(2) site of  $P2_1/n$  polymorphs are surrounded by four Fe<sup>2+</sup> ions that are sitting in the corners of slightly distorted tetrahedra. Such relatively symmetric environments lead to quite small electron-nucleus anisotropy parameters. The Li(1) site of the  $P2_1/n$ polymorph and the Li site within the *Pmnb* polymorph are both bonded to only three Fe<sup>2+</sup> ions and occupy less symmetric positions slightly above triangles of Fe<sup>2+</sup> ions. Li on these sites experiences larger anisotropy of electron-nucleus dipolar interaction. Very similar differences in  $\sigma_{en}^{aniso}$  were observed already for Li nuclei surrounded by either four or three Mn<sup>2+</sup> ions within the Li<sub>2</sub>MnSiO<sub>4</sub> polymorphs [16]. The magnitudes of the anisotropy parameters in LFS and LMS materials are also comparable, suggesting that the BMS effect does not dominate the spinning-sideband patterns. Most likely it affects only intensities of the lowest-rank sidebands (0<sup>th</sup>, 1<sup>st</sup>, 2<sup>nd</sup>), which is probably why the fitting/simulation process in all Li<sub>2</sub>FeSiO<sub>4</sub> polymorphs converged to the values of the assymetry parameter  $\eta_{en}$  of 1.

As in the case of Li<sub>2</sub>MnSiO<sub>4</sub>, the anisotropy parameters thus again reflect the short-range structural motifs of the polymorphs and enable the assignment of two detected NMR

contributions to two lithium sites of the  $P2_1/n$  polymorph. However, the anisotropy parameters of the Li site of the Pmnb polymorph and the Li(1) site of the  $P2_1/n$  polymorph hardly differ from one another. This means that based only on  $\sigma_{en}^{aniso}$  we cannot distinguish between the two Li environments. On the contrary, though centrebands are relatively broad, we can still distinguish different isotropic shifts for the four different lithium sites within the three polymorphs. In the case of the Li<sub>2</sub>MnSiO<sub>4</sub> polymorphs the isotropic shifts were determined by the strength of hyperfine coupling of lithium nuclei with unpaired electronic spins. The hyperfine coupling constants were successfully predicted by DFT projector-augmented-wave (PAW) approach [16], and isotropic shifts obtained from them agreed well with the measured values.

Along the same lines as for the  $Li_2MnSiO_4$  polymorphs, we tried to reproduce the measured isotropic shifts by theoretical calculations also for LFS polymorphs. However, with the available norm-conserving pseudopotentials and within the implemented generalized gradient approximation of Perdew-Burke-Ernzerhof (GGA PBE) the calculated *contact* (hyperfine) isotropic shifts for all four different lithium sites were small and positive. In addition to potential limitations in the accuracy of the first-principles calculations, the discrepancy between the measured and the calculated isotropic shifts in iron containing paramagnetic materials could stem also from the so-called *pseudo-contact* shift. Such a shift can be expected when magnetic susceptibility of a material is anisotropic. Because the aniostropy of magnetic susceptibility or the anisotropy of the g tensor could not be measured in the powdered LFS polymorphs, we again used the GIPAW module of the Quantum Espresso code [29] to predict the anisotropy of tensor g from first principles [31] (based on known crystal structures). When tensor g was obtained, it was inserted into eq. (2), and isotropic pseudocontact shift was then simply calculated as

$$\delta^{PC} = \frac{1}{3} Tr \{ \boldsymbol{\sigma}_{en} \}. \tag{3}$$

Afterwards, the total isotropic shift was obtained as a sum of two contributions, a contact shift and a pseudo-contact shift.

Results of calculations are presented in Figure 9. In all cases pure pseudo-contact shift for lithium nuclei was negative. The magnitude of the pseudo-contact shift was comparable to the magnitude of the contact shift. Although the sum of two contributions in only one case led to a negative total isotropic shift and in three cases led to slightly positive isotropic shifts, the correlation with the measured values is still fine. More importantly, these calculations prove that in case of LFS materials pseudo-contact shifts induced by the anisotropy of tensor g are not negligible and substantially contribute to the total isotropic shift. The calculations also show that rough quantitative estimations of pseudo-contact shifts are possible. To the best of our knowledge, this is the first quantitative analysis of pseudo-contact paramagnetic shifts in lithium based materials.

Quite expectedly, analogous calculations on Li<sub>2</sub>MnSiO<sub>4</sub> polymorphs show that the *g*-tensor anisotropy is negligible in these materials. Since the *g*-tensor anisotropy is directly related to the anisotropy of magnetic susceptibility, it seems reasonable that extensive broadening of centrebands and sidebands observed in <sup>6</sup>Li NMR spectra of the Li<sub>2</sub>FeSiO<sub>4</sub> polymorphs, but not in the spectra of the Li<sub>2</sub>MnSiO<sub>4</sub> polymorphs, is produced by this broadening mechanism. Note the difference between the previously discussed BMS effect and the just mentioned anisotropic bulk magnetic susceptibility (ABMS) effect. The former (BMS) is larger and is important even when magnetic susceptibility tensor is isotropic. It does not affect the width of the centrebands and the sidebands, but, if strong enough, it can affect the intensities of the sidebands, i.e. it can affect the spinning-sideband pattern. The latter (ABMS) mechanism is effective only when magnetic susceptibility tensor is anisotropic. In that case, the ABMS tensors of randomly oriented crystallites around a given crystallite generate a local magnetic field which varies from crystallite to crystallite in the sample. This means that <sup>6</sup>Li nuclei in

different parts of the sample resonate at slightly different frequencies, leading to inhomogeneous line broadening of centrebands and sidebands.

We can roughly estimate the contribution of the ABMS to the width of the NMR signals. VanderHart [B] showed that for an axially symmetric ABMS under MAS the NMR frequencies are spread between  $2\pi(\chi_{\parallel} - \chi_{\perp})/3$  and  $-\pi(\chi_{\parallel} - \chi_{\perp})/3$ . Here  $\chi_{\parallel}$  and  $\chi_{\perp}$  are the parallel and perpendicular components of the volume magnetic susceptibility tensor. For the LFS@900 sample, for which the calculated  ${\it g}$ -tensor is nearly axially symmetric, the calculated difference  $\pi(\chi_{\parallel} - \chi_{\perp})/3$  is equal to 37 ppm. This confirms that linewidths of 60-70 ppm, as detected in LFS samples, indeed stem from ABMS broadening. Unfortunately, linewidths of the  $^6$ Li MAS NMR signals cannot be assessed entirely quantitatively. The extent of the ABMS broadening, namely, does not depend only on the difference  $\chi_{\parallel} - \chi_{\perp}$ , but also on the shape, size, and the packing of the crystallites.

## Carbon-coated Li<sub>2</sub>FeSiO<sub>4</sub> sample

As an example of the application of the above described spectroscopic techniques for the analysis of more demanding materials, carbon-coated  $\text{Li}_2\text{FeSiO}_4$  sample ready for the electrochemical characterisation was studied. The sample was prepared by heat treatment at 700°C, followed by slow cooling to the room temperature. Basically the sample can be described as a LFS@700 sample since its X-ray diffraction pattern (Fig. 10a) is very close to the pattern of the  $\text{Li}_2\text{FeSiO}_4$  crystallized in the  $P2_1/n$  space group (simulated pattern is shown in Fig. 10b). Hardly observable difference between patterns is only in the width of the peaks which are typical for the LFS@700 phase (see arrows in Figs. 10 a and b). This 'imperfections' in the X-ray diffraction pattern are much more pronounced in the Mössbauer spectrum (Fig. 10c). Fit of the spectrum shows that part of iron (58 at.%) has a similar environment as the iron in the LFS@700 sample, whereas another major part of iron (40 at.%) exhibits the QS parameter close to the one of the LFS@400 phase and the IS parameter still

close to the one of the LFS@700 sample. This indicates that phase transformation from the  $P2_1/n$  polymorph to the  $Pmn2_1$  polymorph started but has not yet completed. Similar conclusion can be drawn from the NMR spectrum of the carbon-coated sample (Figure 10d). The spectrum can be described as a sum of two contributions with very similar environments as the ones of the pure LFS@700 phase. However, the ratio of populations of the two lithium sites now deviates from 1:1 and amounts to 0.8:1 (Figure 10d). This suggests that local environment of a substantial part of lithium started to change.

## **Conclusions:**

We showed that <sup>57</sup>Fe Mössbauer and <sup>6</sup>Li MAS NMR spectra were very sensitive to local environment of cations in Li<sub>2</sub>FeSiO<sub>4</sub>, and that the parameters obtained from these spectra were giving typical values for each of the crystallographically pure Li<sub>2</sub>FeSiO<sub>4</sub> polymorphs. The polymorphs differ in the connectivity and in the orientation of the tetrahedra, which together affected the average Fe-O bond lengths, the distortion of the FeO<sub>4</sub> tetrahedra, and the connectivity-scheme between LiO<sub>4</sub> and FeO<sub>4</sub> tetrahedra. Shorter Fe-O bonds had stronger covalent nature and consequently smaller chemical shifts as observed in the Mössbauer spectra. The average Fe-O bond length decreased with the temperature used for the isolation of a particular polymorph (i.e. the shortest bonds were detected in LFS@900 sample, which was obtained by thermally treating the initial sample at 900 °C and quenching it to 25 °C). The asymmetry parameter of the electron-nucleus dipole-dipole interaction, which could be obtained by an analysis of spinning-sideband patterns of <sup>6</sup>Li MAS NMR spectra, depended on the arrangement of Fe<sup>2+</sup> ions around <sup>6</sup>Li nuclei. By inspecting the sideband pattern we could easily discriminate between Li NMR signals that belong to those LiO<sub>4</sub> tetrahedra that only share corners with neighboring FeO<sub>4</sub> tetrahedra, and those LiO<sub>4</sub> tetrahedra that also share an edge with one of the neighboring FeO<sub>4</sub> tetrahedra. Analysis of <sup>6</sup>Li NMR isotropic shifts was

the most demanding. The magnitude and the sign of the shift could not be related plainly to the geometrical description of lithium local environment; the relation between the structure and the isotropic shift was established only by using quantum-mechanical calculations. In the present case of Li<sub>2</sub>FeSiO<sub>4</sub> polymorphs, the isotropic shifts were composed of the contact and the pseudo-contact shift. Based on known structures, both of them were estimated by DFTbased first principles calculations. The calculation of the pseudo-contact shift required knowledge of the components of g-tensor, which were calculated ab-initio using the DFT/GIPAW approach. In Li<sub>2</sub>FeSiO<sub>4</sub> polymorphs the pseudo-contact shifts were of comparable amplitude but of an opposite sign as the contact shifts. The anisotropy of g-tensor was responsible also for severe broadening of NMR signals, which cannot be removed by magic angle spinning. This broadening and the substantial pseudo-contact shift make the analysis of <sup>6</sup>Li MAS NMR spectra of Li<sub>2</sub>FeSiO<sub>4</sub> polymorphs much more demanding than the analysis of NMR spectra of Li<sub>2</sub>MnSiO<sub>4</sub> polymorphs. Spectroscopic investigation of pure Li<sub>2</sub>FeSiO<sub>4</sub> polymorphs, and the knowledge gathered in this way, simplified the analysis of carbon-coated Li<sub>2</sub>FeSiO<sub>4</sub> sample, i.e. it enabled easy identification of deviation from the pure structure.

## **Acknowledgement:**

The financial support from the Ministry of Education, Science and Sport of Slovenia, the Slovenian Research Agency, EN-FIST centre of excellence, CO-NOT centre of excellence and the support from the ALISTORE European Research Institute (ERI) are acknowledged. The Ministère de l'Enseignement Supérieur et de la Recherche, France, is acknowledged for supporting CS through an international PhD student scholarship shared between Amiens (France) and Ljubljana (Slovenia).

## **Figure captions:**

Figure 1: a) TGA curve of pristine hydrothermal LFS sample and b) corresponding normalized DSC data during heating and cooling processes at 10 °C/min under Ar.

Figure 2: Rietveld refinement of the powder X-ray diffraction pattern of LFS@400 (Pmn2<sub>1</sub> space group, a=6.267(4) Å, b=5.335(2) Å, c=4.965(3) Å)

Figure 3: Comparisons between the tetrahedral orientations along equivalent directions in a) LFS@900, in b) LFS@700 and in c) LFS@400.

Figure 4: Mössbauer spectra for a) LFS@900, b) LFS@700 and c) LFS@400 samples.

Figure 5: Relationships between quadrupole splitting (QS) and isomer shift (IS) for LFS polymorphs prepared at different temperatures (only samples without detectable impurities were used in this study).

Figure 6: <sup>6</sup>Li MAS NMR spectra of *Pmn2*<sub>1</sub> (LFS@400 sample), *Pmnb* (LFS@900 sample), and *P2*<sub>1</sub>/n polymorphs (LFS@700 sample). The bottom part of the figure shows entire spectra with broad spinning-sideband patterns. The top part of the figure shows isotropic bands (centrebands) of the three spectra. Spectra of LFS@400 and LFS@900 can be well fitted by a single Li contribution. The spectrum of LFS@700 can be described as a sum of two contributions; one is plotted in green, another in blue. Black solid lines represent measured spectra.

Figure 7: The decomposition of the  $^6$ Li MAS NMR spectrum of the  $P2_1/n$  polymorph (LFS@700) into two contributions. Although the centrebands and the sidebands of the two contributions overlap severely, they produce asymmetric peaks, which still allow relatively reliable decomposition (especially because the spinning-sideband patterns of the two contributions are differently broad and thus the 'asymmetric shape of the peaks' changes with the rank of the sideband).

Figure 8: Calculation of tensors, describing through-space electron-nucleus dipolar interaction. The graph shows the correlation between the measured and the calculated dipolar-interaction anisotropy parameters for four lithium sites in LFS polymorphs.

Figure 9: Correlation between the measured and the calculated (using DFT with PAW reconstruction) contact, pseudo-contact and total isotropic shifts due to electron-nucleus hyperfine and dipolar interactions in LFS polymorphs.

Figure 10: XRD powder pattern (a), simulated XRD pattern (space group  $P2_1/n$ ) (b), <sup>57</sup>Fe Mössbauer spectrum (c), and <sup>6</sup>Li MAS NMR spectrum (d) of the battery sample.

Table 1: Atomic coordinates occupancies and reliability factors obtained by Rietveld refinement of XRD data of electrode composites for LFS@400 (S:G: Pmn2<sub>1</sub>).

LFS@400									
site	Wyckoff	occupancy	X	у	Z				
Li1	4b	1	0.754(2)	0.334(3)	0.988(1)				
Fe1	2a	1	0	0.1740(1)	0.450(2)				
Si	2a	1	0	0.8260(3)	0.966(1)				
O1	2a	1	0	0.8209(3)	0.314(4)				
O2	2a	1	0	0.1147(4)	0.893(3)				
O3	4b	1	0.789(0)	0.6795(1)	0.871(3)				

a=6.2674(6) Å, b=5.3352(7) Å, c=4.9653(5) Å

 $R_f = 6.29\%$ , V/z = 83.013)

Twin mirror at Z=0.956(1) with 0.68 multiplicity of predominant

Table 2: Selected bond lengths and angels of LFS@400 sample

LFS@400								
LiO <sub>4</sub>	O1	O2	О3	О3				
O1	1.992(2)	105.7(4)	107.3(2)	110.8(3)				
O2	3.176(3)	1.991(2)	108.6(2)	113.6(4)				
O3	3.156(1)	3.181(2)	1.925(0)	110.3(2)				
O3	3.238(3)	3.292(1)	3.173(3)	1.941(2)				
SiO <sub>4</sub>	O1	O2	О3	О3				
O1	1.731(1)	104.09(3)	106.53(3)	106.53(3)				
O2	2.614(1)	1.582(1)	114.02(5)	114.02(5)				
O3	2.676(0)	2.674(3)	1.606(3)	110.80(4)				
О3	2.676(0)	2.674(3)	2.644(5)	1.606(3)				
FeO <sub>4</sub>	O1	O2	О3	О3				
01	2.000(2)	101.47(4)	107.49(5)	107.49(5)				
O2	3.273(2)	2.223(2)	104.3(2)	104.3(2)				
O3	3.234(4)	3.346(4)	2.011(0)	128.49(3)				
O3	3.234(4)	3.346(4)	3.622(3)	2.011(0)				

Table 3: NMR parameters\* obtained by the analysis of 6Li MAS NMR spectra

	$oldsymbol{\delta}^{iso}$ [ppm]	$\sigma_{\!en}^{aniso}$ [ppm]	$\eta_{en}$	$\chi_O$ [kHz]	$\eta_O$
LFS@400	-72	800	1.0	24	1.0
LFS@900	-30	-910	1.0	22	0.3
LFS@700 Li1	-7	-920	1.0	21	0.2
LFS@700 Li2	-55	740	1.0	24	1.0

\* $\sigma_{en}^{iso} = Tr(\sigma_{en})/3$ ,  $\sigma_{en}^{aniso} = \sigma_{en}^{izo} - \sigma_{en}^{iso}$ ,  $\eta_{en} = (\sigma_{en}^{YY} - \sigma_{en}^{XX})/\sigma_{en}^{aniso}$ ,  $|\sigma_{en}^{ZZ} - \sigma_{en}^{iso}| \ge |\sigma_{en}^{XX} - \sigma_{en}^{iso}| \ge |\sigma_{en}^{YY} - \sigma_{en}^{iso}|$ ,  $|\sigma_{en}^{ZZ} - \sigma_{en}^{iso}| \ge |\sigma_{en}^{XZ} - \sigma_{en}^{iso}| \ge |\sigma_{en}^{YY} - \sigma_{en}^{iso}|$ ,  $|\sigma_{en}^{ZZ} - \sigma_{en}^{iso}| \ge |\sigma_{en}^{XZ} - \sigma_{en}^{iso}| \ge |\sigma_{en}^{YY} - \sigma_{en}^{iso}|$ ,  $|\sigma_{en}^{ZZ} - \sigma_{en}^{iso}| \ge |\sigma_{en}^{XZ} - \sigma_{en}^{iso}|$ ,  $|\sigma_{en}^{ZZ} - \sigma_{en}^{iso}| \ge |\sigma_{en}^{ZZ} - \sigma_{en}^{iso}|$ ,  $|\sigma_{en}^{ZZ} - \sigma_{$ 

#### **References:**

- [1] Padhi, A.K.; Nanjundaswamy, K.S.; Goodenough, J.B. J. Electrochem. Soc. 1997, 144, 1188.
- [2] Nyten, A.; Abouimrane, A.; Armand, M.; Gustafsson, T.; Thomas, J. O. *Electrochem. Commun.* **2005**, 7, 156.
- [3] Dominko, R.; Bele, M.; Gaberscek, M.; Meden, A.; Remskar M.; Jamnik, J. Electrochem. Commun. 2006, 8, 217.
- [4] Nadherna, M.; Dominko, R.; Hanzel, D.; Reiter, J.; Gaberscek, M., J. Electrochem. Soc., 2009, 156, A619
- [5] Fan, X.-Y.; Li, Y.; Wang, J.-J.; Gou, L.; Zhao, P.; Li, D.-L.; Huang, L.;; Sun, S.-G. J. All. Com., 2010, 493, 77
- [6] Nishimura, S.; Hayase, S.; Kanno, R.; Yashima, M.; Nakayama, N.; Yamada, A. J. Am. Chem. Soc. 2008, 130, 13212.
- [7] Boulineau, A.; Sirisopanaporn, C.; Dominko, R.; Armstrong, A.R.; Bruce, P.G; Masquelier, C. *Dalton Trans.*, **2010**, 39, 6310
- [8] Sirisopanaporn, C.; Boulineau, A.; Armstrong, A.R.; Bruce, P.G.; Hanzel, D.; Budic, B.; Dominko, R.; Masquelier C., *Inorg. Chem.* **2010**, *49*, 7446.
- [9] C. Keffer, A.D. Mighell, F. Mauer, H. Swanson, S. Block, *Inorg. Chem.*, 1967, 6, 119.
- [10] J. Zemann, Acta Crystallographica, 1960, 13, 863
- [11] Menil, F.; J.Phys. Chem. Solids, 1985, 46, 763.
- [12] Grey, C.P.; Dupre, N., Chem. Rev. 2004, 104, 4493.
- [13] Y.J. Lee, C.P. Grey, Chem. Mater. 2000, 12, 3871.
- [14] J. Cabana, J. Shirakawa, G. Chen, T.J. Richardson, C.P. Grey, *Chem. Mater.* **2010**, 22, 1249.
- [15] A.R. Armstrong, C. Lyness, M. Menetrier, P.G. Bruce, Chem. Mater. 2010, 22, 1892.
- [16] Mali, G.; Meden, A.; Dominko, R., Chem. Commun. 2010, 46, 3306.
- [17] Arroyo-deDompablo, M.E.; Dominko, R.; Gallardo-Amores, J.M.; Dupont, L.; Mali, G.; Ehrenberg, H.; Jamnik, J.; Moran, E., *Chem. Mater.* **2008**, *20*, 5574.
- [18] Kunganathan, N.; Islam, M.S., Chem. Mater. 2009, 21, 5196.
- [19] Frayret, C.; Masquelier, C.; Villesuzanne, A.; Morcrette, M.; Tarascon, J.M., Chem. Mater. 2009, 21, 1861.
- [20] Kokalj, A.; Dominko, R.; Gaberscek, M.; Bele, M.; Mali, G., Remskar, M.; Jamnik, J., *Chem. Mater.* **2007**, 19, 3633.
- [21] Carlier, D.; Menetrier, M.; Grey, C.P.; Delmas, C.; Ceder, G., Phys. Rev. B, 2003, 67, 174103.
- [22] Chazel, C.; Menetrier, M.; Carlier, D.; Croguennec, L.; Delmas, C., Chem. Mater. 2007, 19, 4166.
- [23] Carlier, D.; Menetrier, M.; Delmas, C., J. Phys. Chem. C, 2010, 114, 4749.
- [24] Blöchl, P. E., Phys. Rev. B 1994, 50, 17953.
- [25] Carvajal, J. R. An introduction to the program FullProf 2000; at
- http://www.ill.eu/sites/fullprof/php/tutorials.html
- [26] Veshtort, M.; Griffin, R. G.; J. Magn. Reson. 2006, 178, 248.
- [27] Massiot, D.; Fayon, F.; Capron, M.; King, I.; Le Calve, S.; Alonso, B.; Durand, J. O.; Bujoli, B.; Gan, Z. H.; Hoatson, G.; *Magn. Reson. Chem.* **2002**, *40*, 70.
- [28] Perdew, J. P.; Burke, K.; Ernzerhof, M.; Phys. Rev. Lett. 1999, 77, 3865.
- [29] Giannozzi, P.; Baroni, S.; Bonini, N.; Calandra, M.; Car, R.; Cavazzoni, C.; Ceresoli, D.; Chiarotti, G. L.;
- Cococcioni, M.; Dabo, I.; Dal Corso, A.; de Gironcoli, S.; Fabris, S.; Fratesi, G.; Gebauer, R.; Gerstmann, U.;
- Gougoussis, C.; Kokalj, A.; Lazzeri, M.; Martin-Samos, L.; Marzari, N.; Mauri, F.; Mazzarello, R.; Paolini, S.;
- Pasquarello, A.; Paulatto, L.; Sbraccia, C.; Scandolo, S.; Sclauzero, G.; Seitsonen, A. P.; Smogunov, A.; Umari,
- P.; Wentzcovitch, R. M.; J. Phys.: Cond. Matter 2009, 21, 395502. (http://www.quantum-espresso.org).
- [30] Pickard, C.J.; Mauri, F., Phys. Rev. B, 2001, 63, 245101.
- [31] Pickard, C.J.; Mauri, F., Phys. Rev. Lett., 2002, 88, 086403.
- [32] Dominko, R.; J. Power Sources, 2008, 184, 462.
- [33] Keffer, C.; Mighell, A.D.; Mauer, F.; Swanson, H.; Block, S.; Inorganic Chemistry. 1967, 6, 119.
- [34] Rodriguez-Carvajal, J., Phys. Rev. Lett., 1998, 21, 4660.
- [35] Sirisopanaporn, C.; Masquelier, C.; Armstrong, R.A.; Dominko, R.; submitted 2010.
- [36] Dyar, M.D.; Perry, C.L.; Rebbert, C.R.; Dutrow, B.L.; Holdaway M.J.; Lang, H.M.; Am. Miner., 1991, 76, 27.
- [37] Quoirin, G. PhD thesis, Universite de Picardie Jules Verne 2007.
- [38] Communicated orally by A. Yamada et al. during the LiBD (Lithium Battery Discussion) Meeting held in Arcachon (FRANCE) in September 2009.
- [39] Nayeem, A.; Yesinowski, J.P.; J. Chem. Phys. 1988, 89, 4600.
- [40] Ashcroft, N.W.; Mermin, N.D.; Solid State Physics, Saunders College Publishing, Fort Worth, 1976.
- [41] Lee, Y.J.; Grey, C.P. J. Phys. Chem. B 2002, 106, 3576.
- [42] VanderHart, D.L.; Earl, W.L.; Garroway, A.N. J. Magn. Reson. 1981, 44, 361.

[43] Kubo, A.; Spaniol, T.P.; Terao, T. J. Magn. Reson. 1998, 133, 330.